# Supporting Online Material for

## Patches with Links: A Unified System for Processing Faces in the Macaque Temporal Lobe

Sebastian Moeller, Winrich A. Freiwald, Doris Y. Tsao*

*To whom correspondence should be addressed. E-mail: doris@nmr.mgh.harvard.edu

Published 6 June 2008, *Science* **320**, 1355 (2008)
DOI: 10.1126/science.1157436

**This PDF file includes**

# Patches with Links: A Unified System for Processing Faces in the Macaque Temporal Lobe

Sebastian Moeller, Winrich A. Freiwald, Doris Y. Tsao

## Supporting Online Material

## Materials and Methods

All animal procedures complied with the NIH Guide for Care and Use of Laboratory Animals, regulations for the welfare of experimental animals issued by the Federal Government of Germany, and stipulations of Bremen authorities.

**Overview.** Four male rhesus macaques were implanted with MR-compatible headposts and trained to fixate for a juice reward both inside and outside the scanner. After initial training, face-selective cortical areas were localized using fMRI. Then MR-compatible recording chambers were implanted to allow access to specific face patches in each monkey. The face selectivity of cells inside and outside the face patches was characterized by extracellular recordings to confirm successful targeting. We then stimulated specific sites inside the scanner, while the animal fixated a small fixation cross over a gray background for juice reward. See (*1, 2*) for details on fMRI procedures and (*3*) for details on fMRI-guided targeting and extracellular recording procedures.

**Surgery.** Surgical procedures followed standard anesthetic, aseptic, and postoperative treatment protocols which have been described in detail elsewhere (*4*). The headpost was implanted in two surgical procedures separated by several weeks recovery time. First, the monkey was anesthetized (Ketamin / Medetomidine, 8mg/kg / 0.04mg/kg), then intubated and switched to a maintenance regime of oxygen (30 %), nitrous oxide (70 %) and isoflurane (0.5-2 %). The monkey's head was postioned in a stereotaxic frame, and the skull was exposed and cleaned (peroxide 30% and saline). Projections of the

estimated chamber border and headpost were marked on the skull, and positions for 20 ceramic screws were marked. After drilling and thread cutting, the screws were inserted and covered with several layers of acrylic cement, as was all of the exposed skull area. Anesthesia was ended and the monkey was given a period of six weeks or longer to recover. In a brief second surgery, an MR-compatible headpost was attached to the initial implant using acrylic cement.

After computing the chamber location and angle allowing access to the desired face patch, we implanted the recording chamber using the same two-step anesthesia regime described above. A Cilux chamber was positioned using a stereotaxic frame and custom-made manipulators that allowed us to specify the center position of the chamber on the skull as well as rotation and tilt. The chamber was fastened using acrylic cement.

Prior to extracellular recording, a craniotomy was made inside the chamber under Ketamin / Medetomidine anesthesia; the diameter of the craniotomy was initially kept small and was enlarged as required.

**Monkey fMRI.** All scanning was performed on a 3T MR scanner (Allegra, Siemens). For each monkey we acquired 10 anatomical volumes at high spatial resolution (0.5 mm isometric) for surface reconstruction and activity visualization. We used a T1 weighted inversion recovery sequence (MPRAGE). These scans were performed under Ketamin / Medetomidine anesthesia to reduce motion artifacts.

For all functional imaging, a contrast agent, ferumoxtran-10 (Sinerem, Guerbet; concentration: 21 mg Fe/ml in saline; dosage: 8 mg Fe/kg) was injected into the femoral vein prior to each scan session. Sinerem is the same compound as MION, produced under a different name (*5*). Sinerem/MION increases signal-to-noise and gives finer spatial localization than BOLD (*6, 7*).

Unlike BOLD, Sinerem results in a signal reduction at activated voxels; for all presented functional data we inverted the signal, to allow easy comparison to BOLD data. All functional data was acquired in coronal slices. We used a multi-echo sequence (EPI, TR 3 or 4 s, TE 30 or 25 ms, 64 x 64 matrix). In combination with a concomitantly acquired fieldmap, this allowed high fidelity reconstruction by undistorting most of the B0-field inhomogeneities (*8, 9*).

For the initial fMRI experiment to localize face patches, we used a block design. Data for each animal was acquired over several scan sessions (M1: 15 runs in 2 sessions, M2: 18 runs in 3 sessions, M3: 35 runs in 3 sessions, M4: 23 runs in 3 sessions). In these localizer experiments we acquired 136 volumes per run (28 slices, spatial resolution 1.25 mm isometric, TR 4 s). The slice volume was adjusted for each monkey to cover the temporal lobe.

For all microstimulation experiments (with the exception of the experiment shown in supplementary text), the monkey fixated a small cross (0.36° diameter) on a plain gray background for a juice reward. We used either 21 slices at 1.25 mm isometric resolution (TR 3 s, block length 30 s, 170 volumes/run), or 28 slices at 1.5 mm isometric resolution (TR 4 s, block length 32 s. 136 volumes/run, or TR 3 s, block length 30 s, 170 volumes/run), or 42 slices at 1.5 mm isometric resolution (TR 4 s, block length 32 s, 136 volumes/run); the last prescription covered almost the whole brain.

In the experiment combining external visual stimuli with electrical microstimulation (supplementary text) we used the following scan parameters: 28 slices at 1.5 mm isometric resolution, TR 3 s, 200 volumes / run.

**Targeting the face patches.** Targeting of face patches required a two-step procedure: 1) computing the skull position and orientation of a recording chamber to allow access to the face patch, and 2) computing which grid angle and grid hole to use within the

chamber. To accomplish step 1, we used a custom MATLAB program to position a virtual chamber such that it would reach the desired face patch and the rim of the chamber would lie over the skull. This yielded coordinates specifying the center of the chamber axis on the skull as well as two angles for this axis (in the coronal and sagittal planes; in most instances the angle in the sagittal plane was 0°). To accomplish step 2, we acquired an anatomical scan of the monkey's brain with a recording grid positioned inside the cylinder whose holes were filled with MR-visible silicone. Registering the face patch localizer data to this anatomical scan allowed us to determine which grid hole to use to reach the desired face patch. The use of angled grids allowed us to reach face patches lying outside the direct projection of the chamber. Thus, for example, we were able to target four different face patches (ML, AL, AM, and AF) from the same recording chamber in monkey M1.

**Electrophysiological recording.** We used standard non-magnetic tungsten electrodes (FHC) of low impedances (0.5 or 1 MΩ at 1 kHz). To allow scans of the electrodes *in situ* we used MR-compatible grids and guidetubes. We used a tungsten rod as indifferent electrode, which we lowered into the saline-filled grid and chamber. A custom all-plastic advancer was used to advance the electrode.

Extracellular signals were amplified and fed into a dual window discriminator to separate up to two units. The low impedance stimulation electrodes almost exclusively recorded multi-unit activity. Spikes were stored as time stamps at a temporal resolution of 1 ms.

**Microstimulation.** To map the connectivity of the face patches, we stimulated pre-targeted sites in the temporal lobe. The stimulation protocol followed a block design. We normally interleaved 9 blocks of fixation-only with 8 blocks of fixation plus electrical microstimulation; we always started and ended with a fixation-only block. During

microstimulation blocks we applied one pulse train per second, lasting 200 ms with a pulse frequency of 300 Hz. Bipolar current pulses were charge balanced, with a phase duration of 300μs and a distance between the two phases of 150μs. In the early phase of the project, we used a nominal current amplitude of 100 μA; we later switched to 300 μA since this yielded stronger activations. Due to the capacity of electrode and cable, only ~ 50-90 % of the nominal charge was actually delivered into the tissue (the unloading of this capacity could be observed as an inverted current at the end of each rectangular half-pulse on the control oscilloscope).

We used a programmable constant voltage impulse generator to drive a constant current stimulus isolator, which interfaced with different and indifferent electrodes through a coaxial cable. All stimulus generation equipment was stored in the scanner control room; the coaxial cable was passed through a wave guide into the scanner room.

**Visual stimulation.** We used four visual stimulation protocols, one for unit characterization and three for MRI experiments. In all protocols the monkey's task was to maintain fixation on a central fixation spot (0.36° diameter); the required fixation duration to earn a drop of juice was lowered from 4 s to 1 s in each session. Gaze was measured in all experiments using an infra-red based system.

Face patch localizer: The face patch localizer stimulus followed a block design. Blocks lasted 32 seconds, and included the following image categories: human faces (F), monkey faces (M), hands (H), gadgets (G), fruits and vegetables (V), and headless human bodies (B). There were 16 different images in each category. Each image block was preceded by a block consisting of scrambled versions of the same images (S), resulting in the following sequence: S F S H S M S G S F S V S M S B R (the final block consisted of a gray random dot pattern). Each image subtended 12° visual angle (10.4 cm diameter at 49 cm distance), and was presented for 0.5 s.

Unit characterization: For electrophysiological recordings, we used a set of 128 images representing 8 different categories (16 images per category): faces, fruits and vegetables, gadgets, hands, headless human bodies, monkey body parts, headless monkey bodies, and finally, block-scrambled images. The images measured 100 x 100 pixels and spanned 7.6° visual angle (6 cm diameter at 45 cm distance). The images were presented in random sequence (duration 200 ms followed by 200 ms of gray background).

Microstimulation without visual stimulation: To keep the animals awake and fixating during pure microstimulation sessions (i.e., all microstimulation experiments except that shown in supplementary text), we presented a fixation spot on a plain gray background through the experiment.

Microstimulation with visual stimulation: For the experiment shown in the supplementary text, we combined visual and microstimulation. Visual stimulation consisted of faces (F, 64 images), objects (O, 32 images, 16 gadgets and 16 fruits and vegetables), and pure gray (G, full screen). Stimuli followed the sequence: G (60), F (30), G (60), F* (30), G (60), O (30), G (60), O* (30), G (60), G (30), G (60), G* (30), G (60) (duration in seconds indicated after each block, the asterisk indicates that electrical stimulation was also applied). Each image subtended 12° visual angle.

During MRI sessions, visual stimulation was performed using custom code utilizing the Psychophysics Toolbox (*10*). The stimuli were displayed at 60 Hz with a resolution of 1280 x 1024 pixels, using a video beamer and a back projection screen. During unit characterization outside the scanner, visual stimulation was performed using RF3 (a custom data acquisition program designed by the late David Freeman and by Margaret Livingstone). Stimuli were displayed at 60 Hz with a resolution of 640 x 480 pixels.

**Electrophysiological data analysis.** To compute the selectivity profile of recorded single- and multi-units, we sorted the recorded data by image category, calculated the

mean activity to each category (over 100 ms, starting 100 ms after onset) and then subtracted the mean baseline activity (the mean activity during the first 75 ms after stimulus onset). If the response of a unit to faces was at least twice as large as that to the next-best category, we considered it to be face selective. Only data obtained during stimulus presentations in which the monkey's eye position was within a window of +/- 4.5° around the fixation spot for at least 95% of the presentation duration (to allow for blinks) was analyzed.

**fMRI data analysis.** We used FreeSurfer (http://surfer.nmr.mgh.harvard.edu) to reconstruct cortical surfaces and to create flat representations of each monkey's visual cortex, as if sampled at the cortex-white-matter boundary. The resulting flatmaps give an overview of the spatial distribution of fMRI activation maps.

We used FS-FAST for functional data analysis. Table S1 summarizes the number of runs used to generate each of the figures presented in the paper. Runs in which there was excessive motion were discarded. Data were motion-corrected with the AFNI motion correction algorithm (*11*), and intensity normalized. This preprocessed data was then analyzed using a generalized linear model (GLM) approach. To define face-selective areas we calculated the contrast faces versus all other objects (without scrambled images). To define areas activated by microstimulation, we contrasted activity during microstimulation epochs versus fixation-only epochs. All color scale bars show the significance of the contrast maps as negative common logarithm of the probability of error.

Each monkey's face localizer data was used to generate a mean functional volume, which defined the common functional space for the monkey. All subsequent functional data was registered to this common functional space using a custom registration program

(written by Joe Mandeville), and all regions of interest (ROIs) were defined in this common functional space.

Mean time courses from each ROI were extracted using custom Matlab code. The mean time series across all voxels within the ROI was detrended with a second order polynomial. To analyse the interaction between visual and electrical microstimulation, we extracted the mean GLM beta values (scaled to percent signal change) for all voxels of each ROI.

To analyze the data presented in the supplementary text, we only included volumes recorded at time points during which the monkey kept his gaze inside a window +/- 3 degrees around the fixation spot for at least 80% of the TR length (to allow for blinks); to account for hemodynamic delay, we assumed that affected volumes were delayed by 5 s.

## Supplementary Text: Effect of combining visual and electrical stimulation

To test for interactions between visual and electrical stimulation, we combined the two in a stimulus sequence composed of six conditions: faces, faces + microstimulation, objects, objects + microstimulation, blank, and blank + microstimulation. We ran two monkeys on this stimulus sequence, microstimulating in ML. Supplementary Text Figure 1 shows the fMRI activation to these six conditions within each of the six face patches in monkey M1.

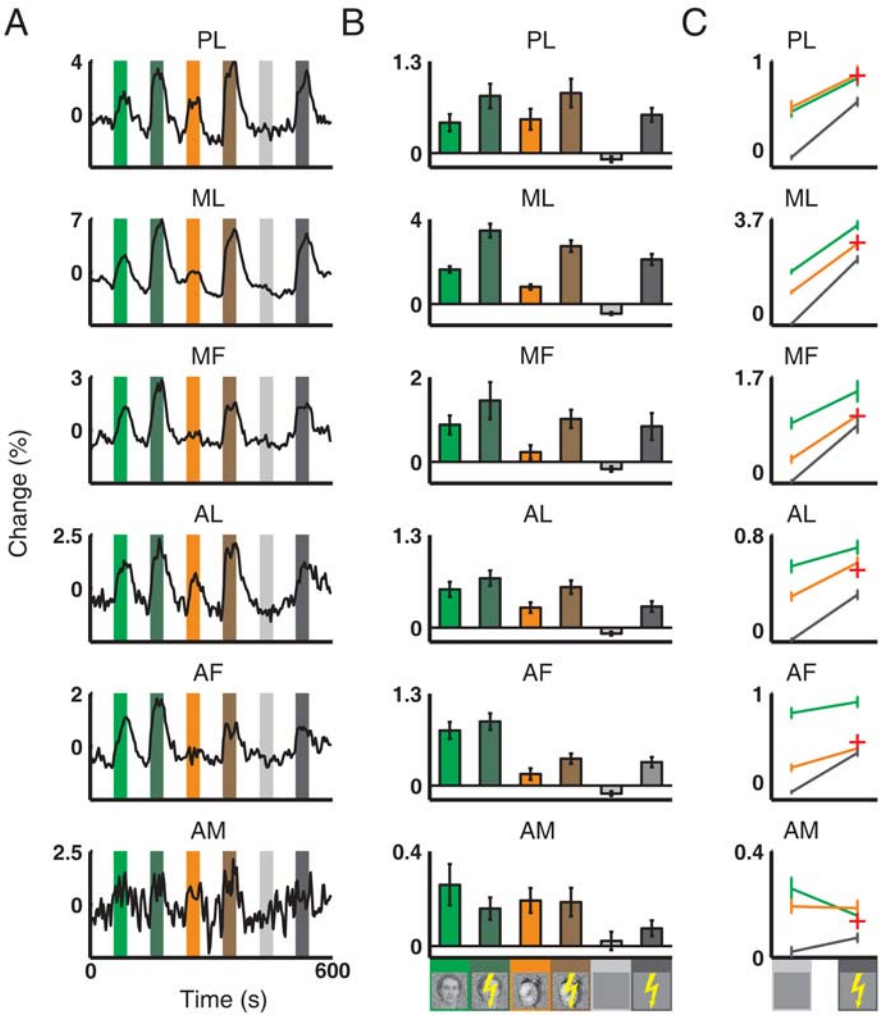

***Supplementary Text Figure 1. Effects of combining visual and electrical stimulation.*** ***(A)*** *Average time course from each face patch ipsilateral to the stimulated hemisphere. The color code for the six conditions (faces, faces and microstimulation, objects, objects and microstimulation, blank, blank and microstimulation) is given below the bar graphs in (B). The time course from AM was noisy due to signal extinction at the temporal pole in this experiment.* ***(B)*** *Mean activation to the six stimulation conditions (error bars indicate 95 % confidence intervals).* ***(C)*** *Activation to blank, faces, and non-face objects, with (right) and without (left) microstimulation (same data as (B), plotted in a different format). The "+" indicates the predicted level of activation to objects plus microstimulation, assuming a model in which visual and electrical stimulation exert independent effects.*

The results appear qualitatively consistent with a model of independent effects of visual and electrical stimulation, since activity in PL, ML, MF, AL, and AF increased during microstimulation epochs, regardless of whether the monkey was viewing faces, objects, or a blank screen (Supplementary Text Figure 1). ANOVA analysis with two factors (visual stimulation condition and microstimulation condition) showed that both main effects were highly significant in all face patches, with the exception of the effect of microstimulation in AM (due to poor signal-to-noise ratio in the region of AM in this experiment). The ANOVA analysis revealed only weak interactions between visual and electrical stimulation that reached significance in only two patches at $p = 0.01$ (p values indicated in the table below).

| Patch | Significance of microstimulation | Significance of visual stimulation | Significance of interaction |
|---|---|---|---|
| AF | $p<<0.001$ | $p<<0.001$ | $p=0.0008$ |
| AL | $p<<0.001$ | $p<<0.001$ | $p=0.03$ |
| AM | $p=0.39$ | $p<<0.001$ | $p=0.02$ |
| MF | $p<<0.001$ | $p<<0.001$ | $p=0.16$ |
| ML | $p<<0.001$ | $p<<0.001$ | $p=0.002$ |
| PL | $p<<0.001$ | $p<<0.001$ | $p=0.1$ |

Below, we assume a model of independent effects to estimate the fraction of neurons activated by visual versus electrical stimulation.

A model of independent effects of visual and electrical stimulation: Let us assume: 1) that visual and electrical stimulation activate independent fractions of neurons, and 2) that a neuron's state is binary, i.e., activated or not activated (although not essential, this assumption simplifies the equations). Let M denote the maximal activation of a face patch, let B, O, and F denote activations to a blank screen, objects, and faces, respectively, in the absence of microstimulation, and let B*, O*, and F* denote corresponding activations to visual stimuli in the presence of microstimulation.

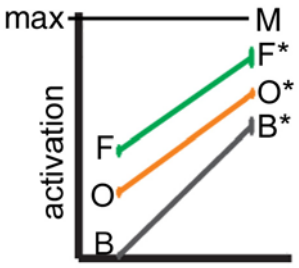


Each activation value can be expressed as a fraction of the theoretical maximum, M:

$$\begin{aligned} B &= f_1 \times M \\ B^* &= f_2 \times M \\ O &= f_3 \times M \\ O^* &= f_4 \times M \\ F &= f_5 \times M \\ F^* &= f_6 \times M \end{aligned} \qquad (1)$$

If electrical and visual stimulation are fully independent, then the activity elicited in response to combined visual and electrical stimulation can also be described using the following formulas:

$$\begin{aligned} O^* &= \left(f_2 + f_3 - \left(f_2 \times f_3\right)\right) \times M \\ F^* &= \left(f_2 + f_5 - \left(f_2 \times f_5\right)\right) \times M \end{aligned} \qquad (2)$$

This is because activated fractions are independent (see figure below); the subtraction term ensures that the fraction of neurons activated by both visual and electrical stimulation is counted only once.

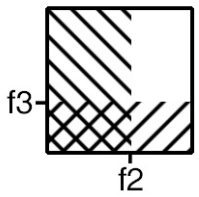


Combining equations (1) and (2) yields five equations in four unknowns ($f_2$, $f_3$, $f_5$, M):

$$\begin{aligned} B^* &= f_2 \times M \\ O &= f_3 \times M \\ F &= f_5 \times M \\ F^* &= \left(f_2 + f_5 - \left(f_2 \times f_5\right)\right) \times M \\ O^* &= \left(f_2 + f_3 - \left(f_2 \times f_3\right)\right) \times M \end{aligned} \qquad (3)$$

Combining the first four equations in (3) yields:

$$F^* = \left(\frac{B^*}{M} + \frac{F}{M} - \left(\frac{B^*}{M} \times \frac{F}{M}\right)\right) \times M \qquad (4)$$

which can be rearranged into:

$$M = \frac{B^* \times F}{B^* + F - F^*} \qquad (5)$$

Thus M can be computed from experimentally measured values for B*, F, and F*. Then, $f_2$, $f_3$, and $f_5$ can be computed using the first three equations in (3). Finally the model allows us to *predict* a value for O* using the last equation in (3).

To obtain values for O, F, B*, O*, and F*, we extracted the mean hemodynamic response strength for the six patches to the six different stimulation conditions

(Supplementary Text Figure 1B). We then used these measurements to compute predicted values of $f_2$, $f_3$, $f_5$, M, and O*, as outlined above.

The following table summarizes the results of these computations. The subscript *m* denotes measured values, the subscript *c* denotes computed values, and the subscript *p* denotes the predicted value. All values are scaled to percent signal change, except the three values f2, f3, f5, which are unit-less fractions of the maximum M.

| Patch | $B^*_m$ | $O_m$ | $F_m$ | $F^*_m$ | $f2_c$ | $f3_c$ | $f5_c$ | $M_c$ | $O^*_m$ | $O^*_p$ |
|---|---|---|---|---|---|---|---|---|---|---|
| AF | 0.33 | 0.16 | 0.78 | 0.90 | 0.26 | 0.13 | 0.62 | 1.25 | 0.38 | 0.45 |
| AL | 0.30 | 0.28 | 0.54 | 0.70 | 0.26 | 0.25 | 0.47 | 1.15 | 0.57 | 0.51 |
| AM | 0.07 | 0.19 | 0.26 | 0.16 | 0.68 | 1.76 | 2.37 | 0.11 | 0.19 | 0.14 |
| MF | 0.84 | 0.23 | 0.87 | 1.45 | 0.30 | 0.08 | 0.32 | 2.76 | 1.01 | 1.00 |
| ML | 2.10 | 0.80 | 1.63 | 3.47 | 0.16 | 0.06 | 0.13 | 12.78 | 2.73 | 2.77 |
| PL | 0.54 | 0.48 | 0.43 | 0.81 | 0.38 | 0.33 | 0.30 | 1.43 | 0.85 | 0.84 |

Predicted values of $O^*$ (indicated by +'s in Supplementary Text Figure 1C) always fell close to actually measured values, demonstrating the consistency of the model with experimental results. The paradoxical values computed for AM reflect the fact that microstimulation of ML did not produce significant activation in AM in this experiment. Discounting the results from AM, the fraction of neurons activated by microstimulation ($f2_c$, mean = 0.27) was always larger than that activated by viewing non-face objects alone ($f3_c$, mean = 0.17), and in several cases comparable to that activated by viewing faces alone ($f5_c$, mean = 0.37).

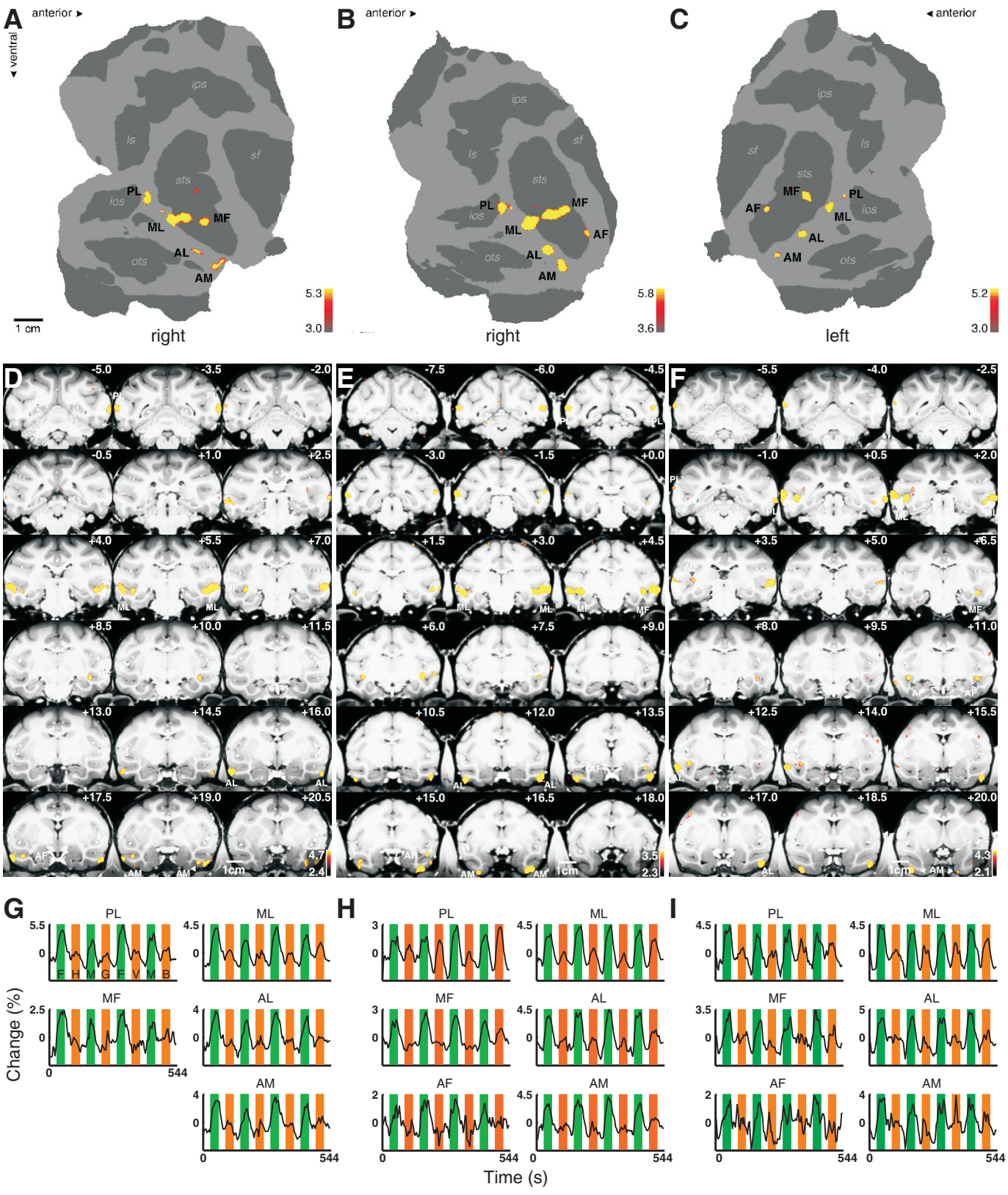


Figure S1: the face patches (M2, M3, M4)

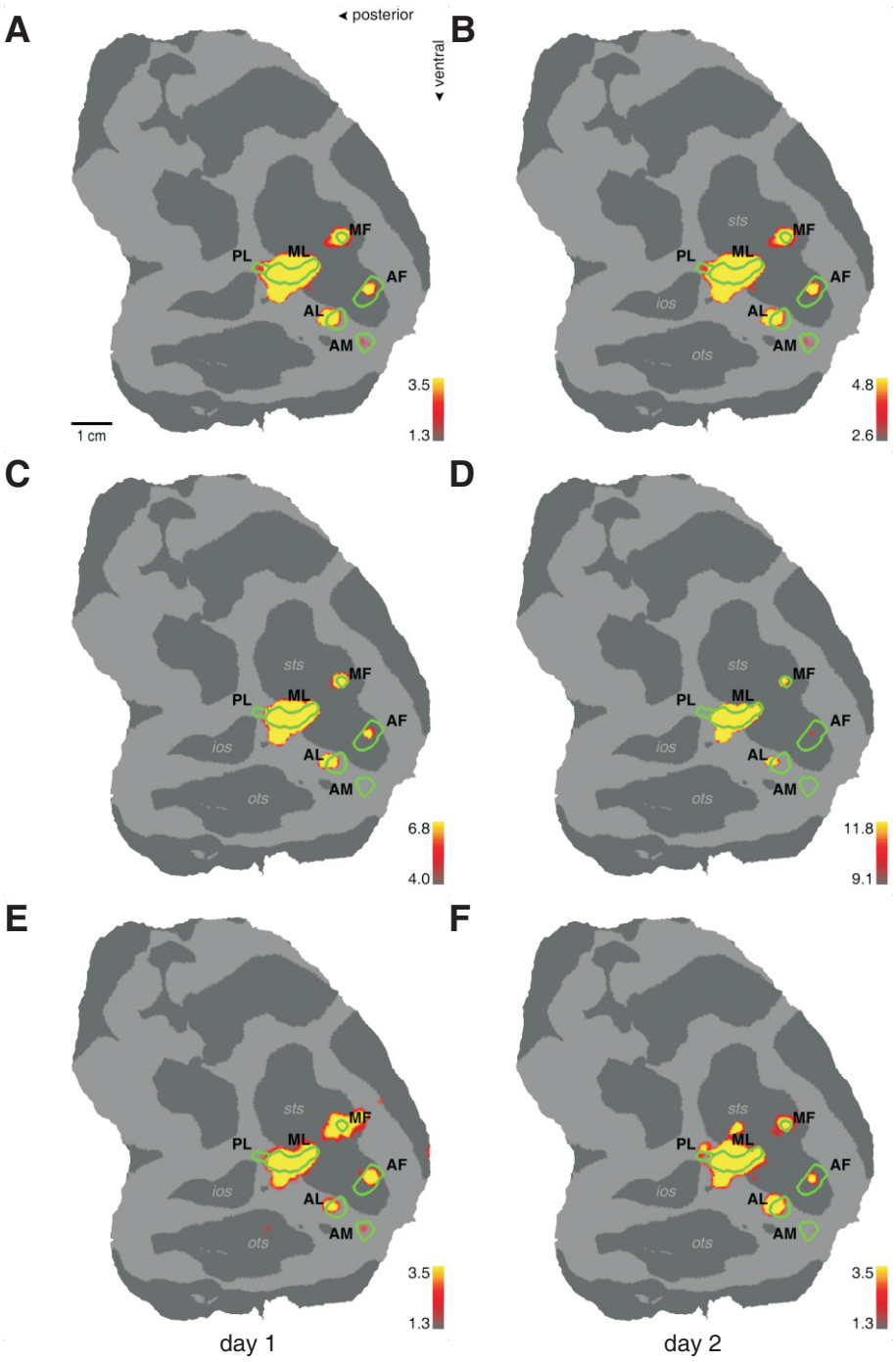


Figure S2: robustness and reproducibility (stimulation inside ML, M1)

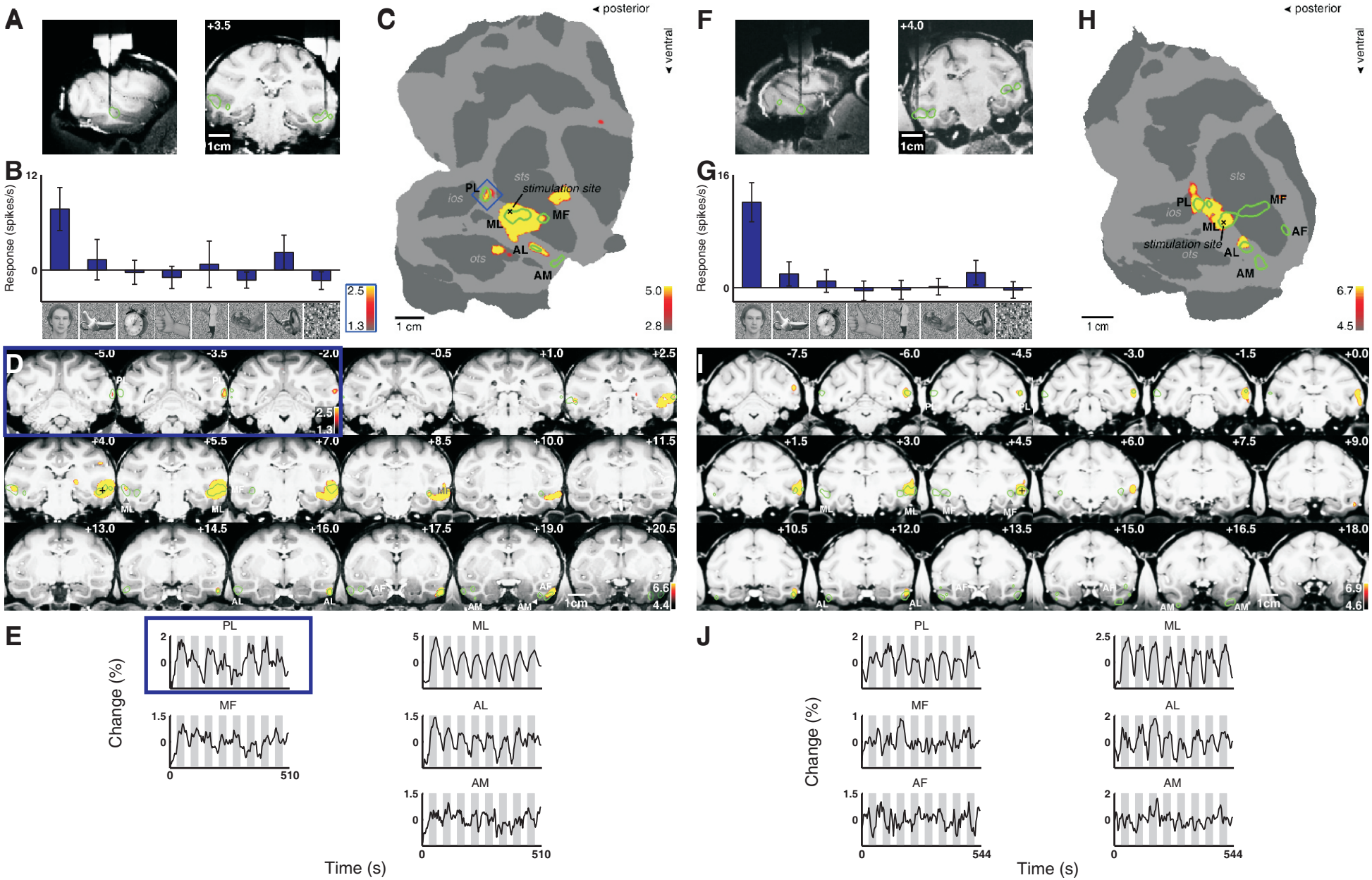


Figure S3: stimulation inside ML (M2, M3)

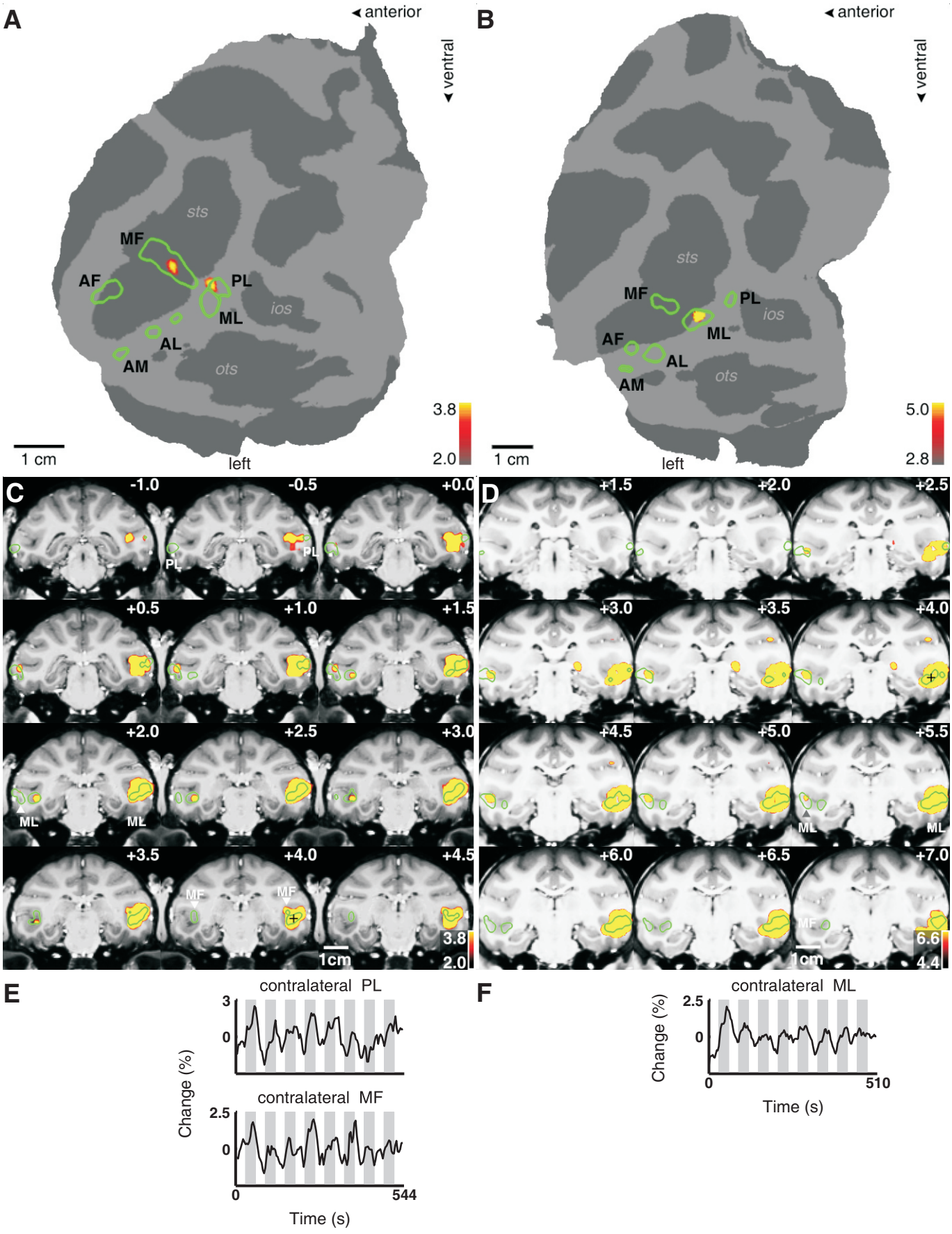


Figure S4: contralateral activation by stimulation inside ML (M1, M2)

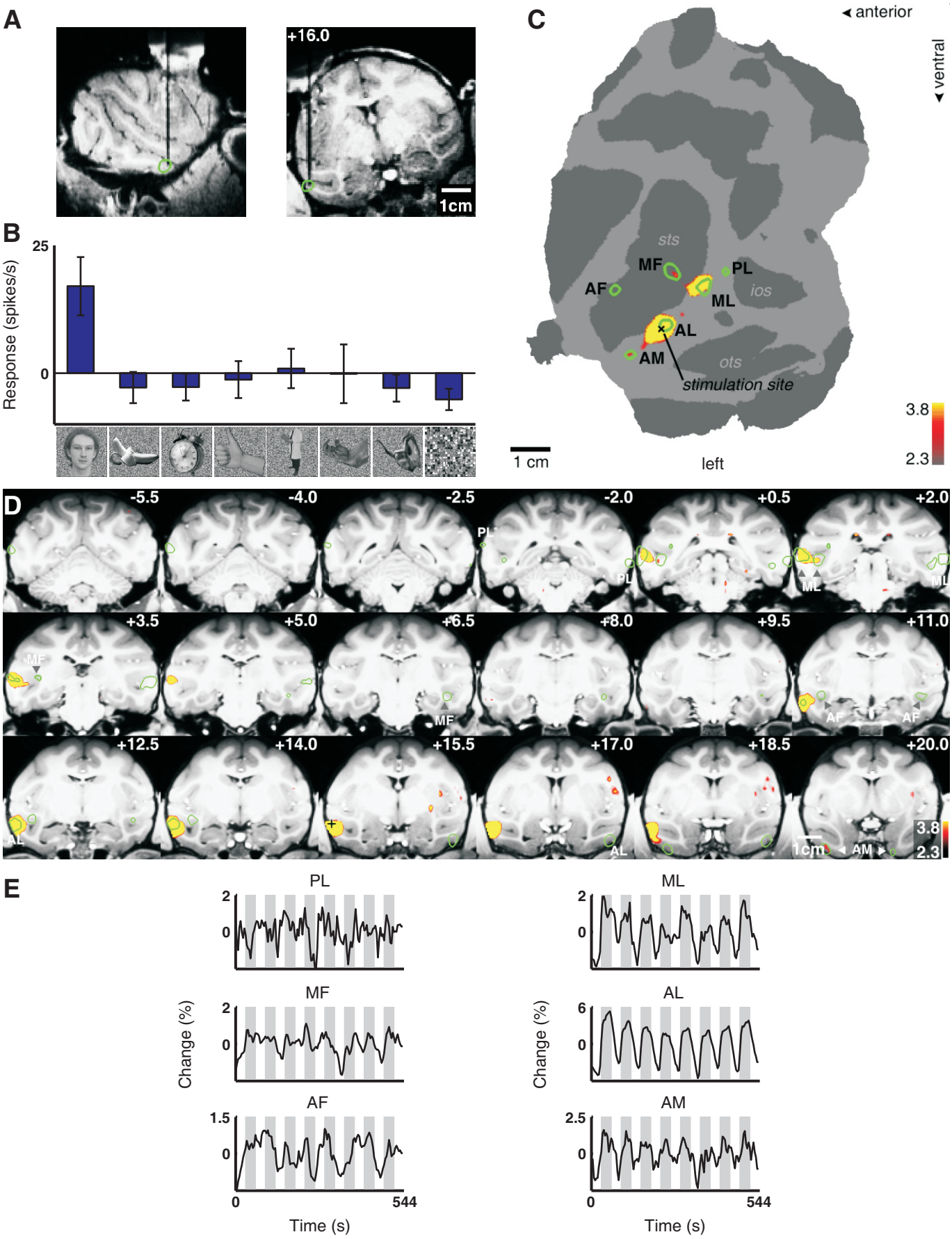


Figure S5: stimulation inside AL (M4)

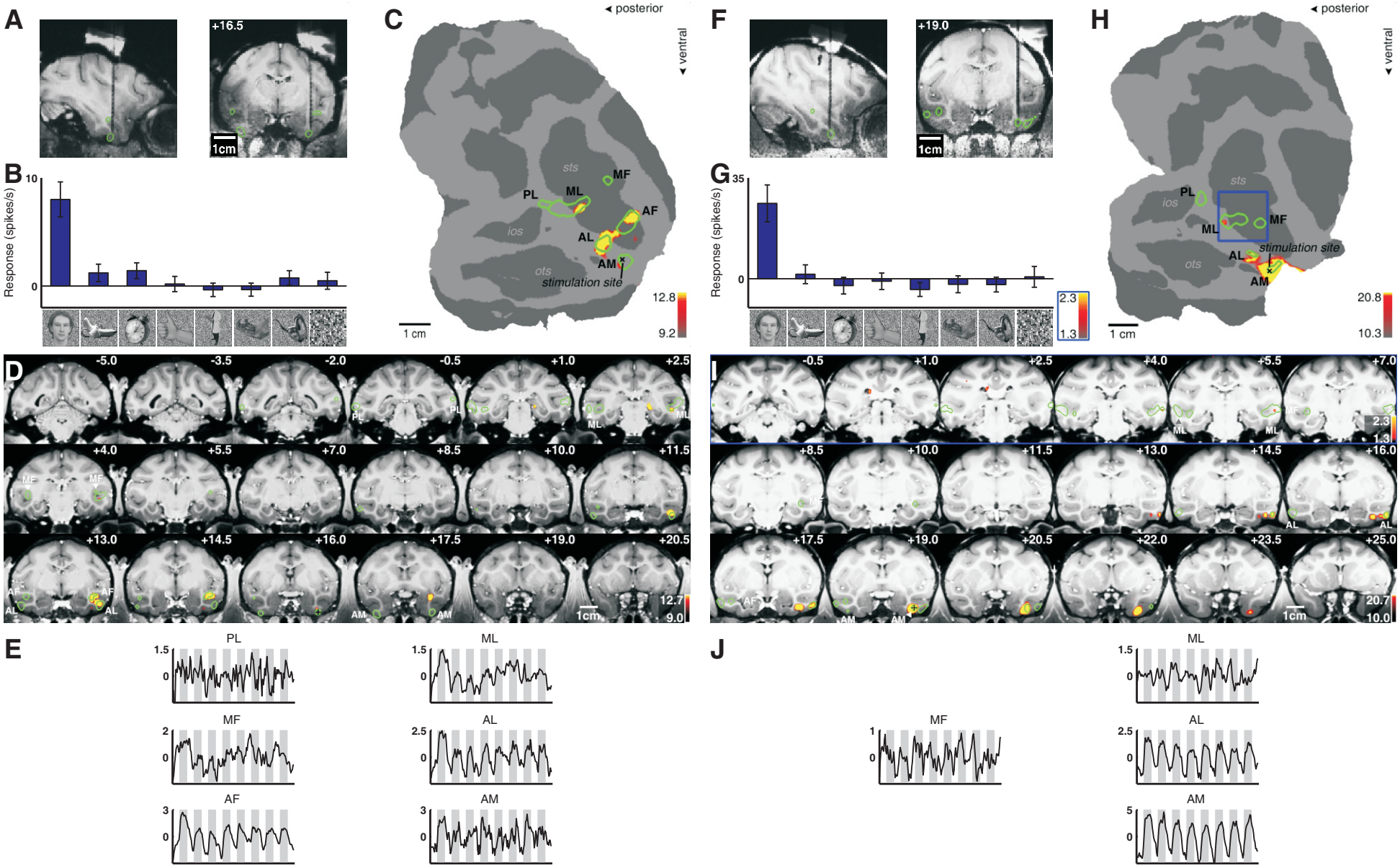


Figure S6: stimulation in AM (M1, M2)

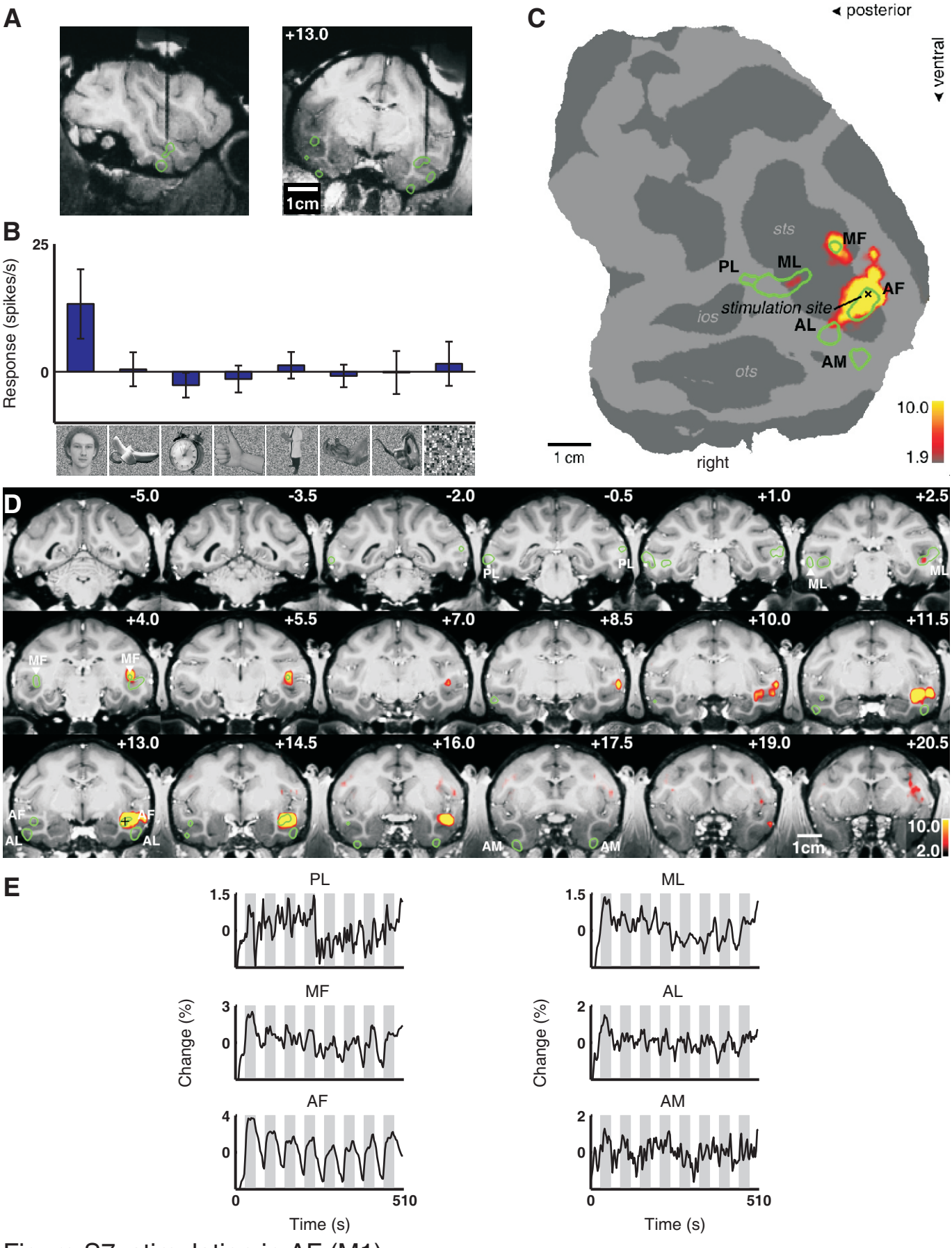


Figure S7: stimulation in AF (M1)

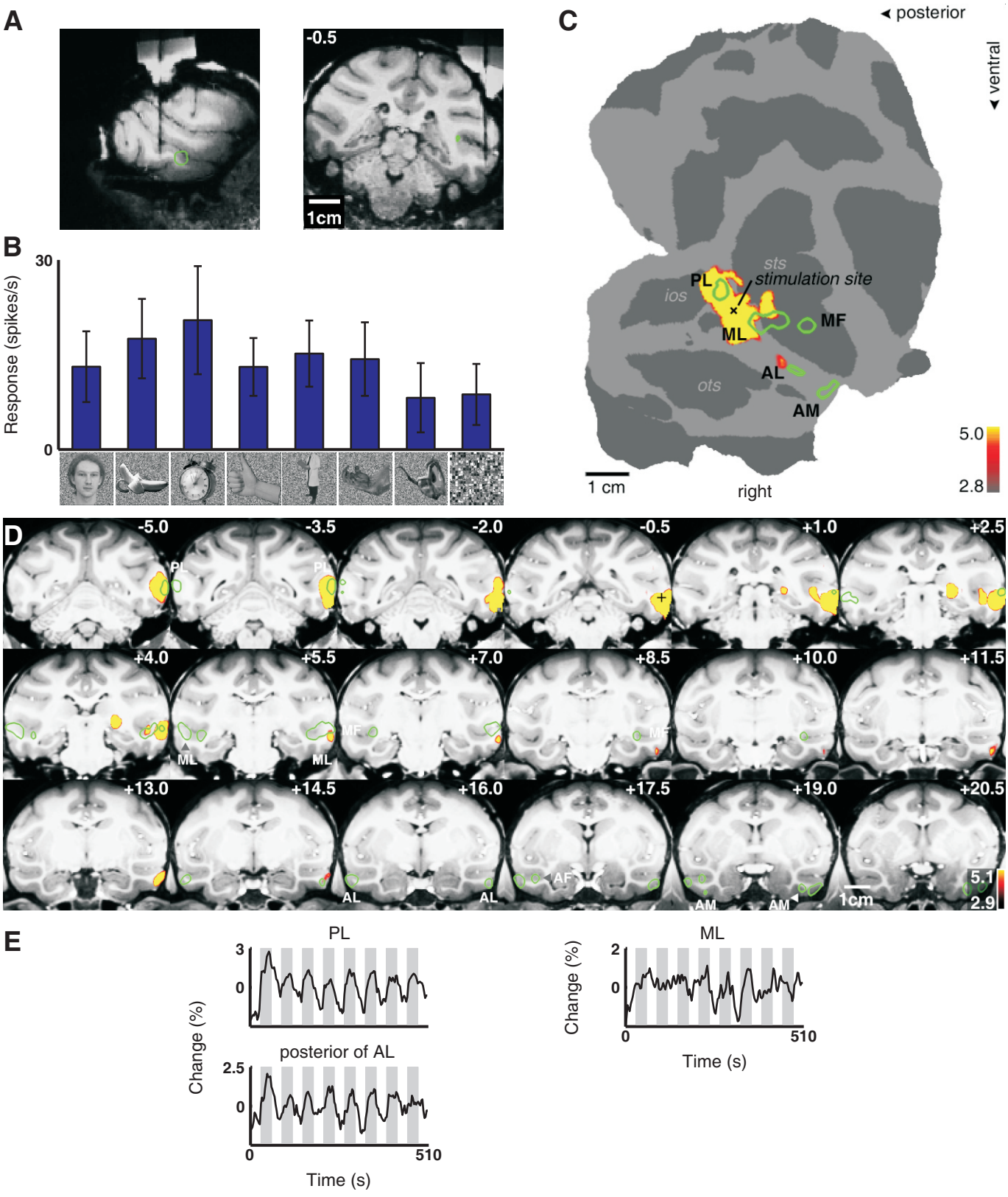


Figure S8: stimulation outside ML (M2)

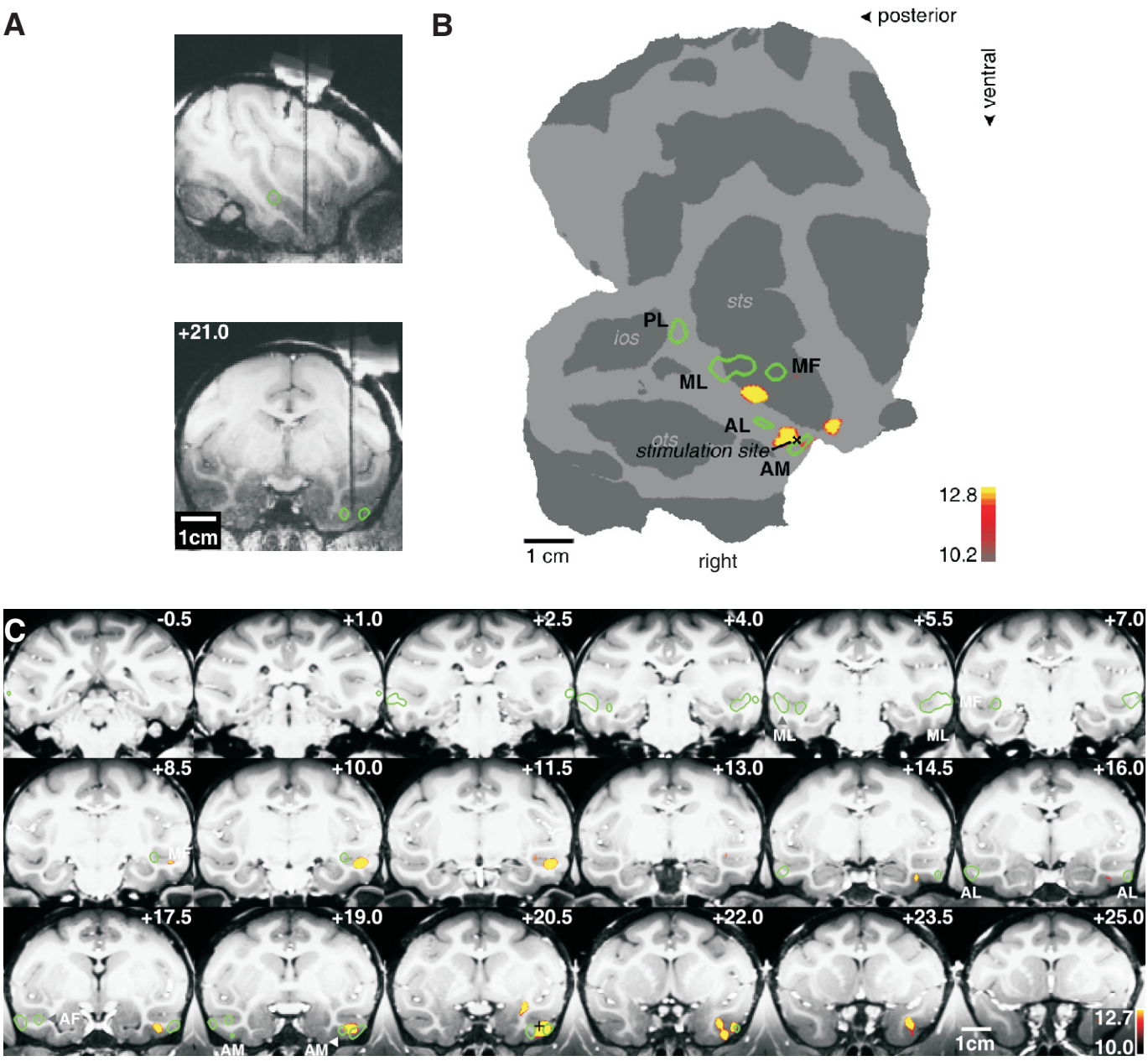


Figure S9: stimulation outside AM (M2)

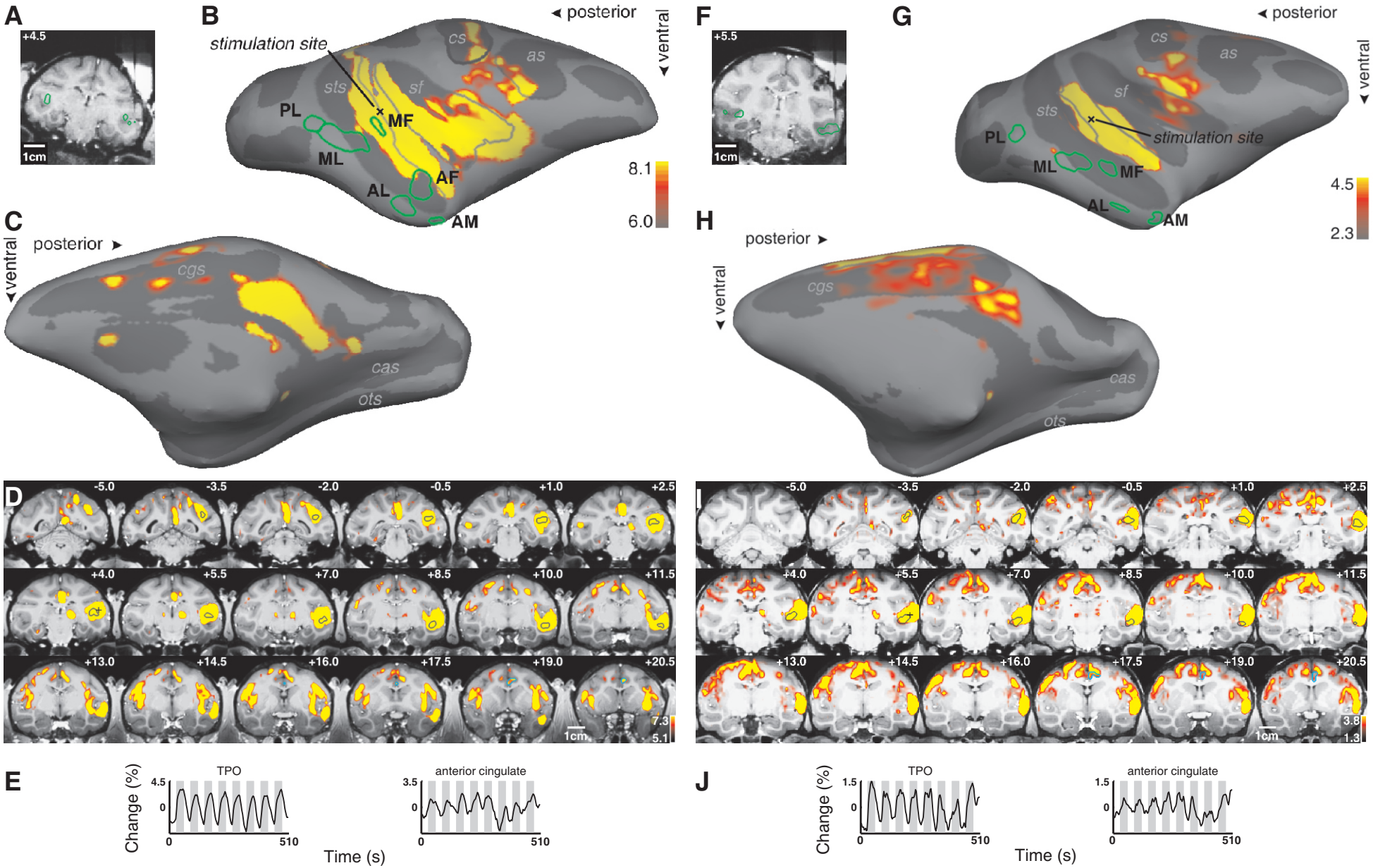


Figure S10: stimulation inside dSTS (M1, M2)

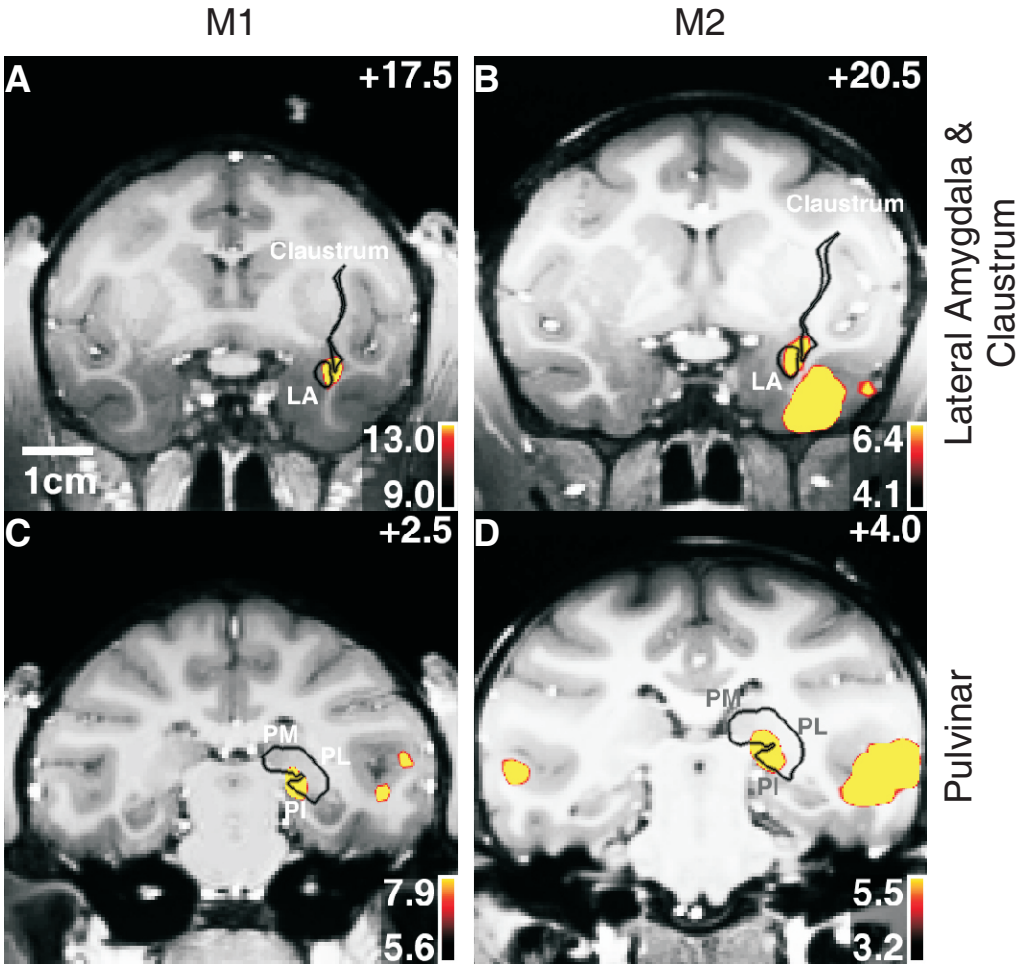


Figure S11: subcortical projections (M1, M2)

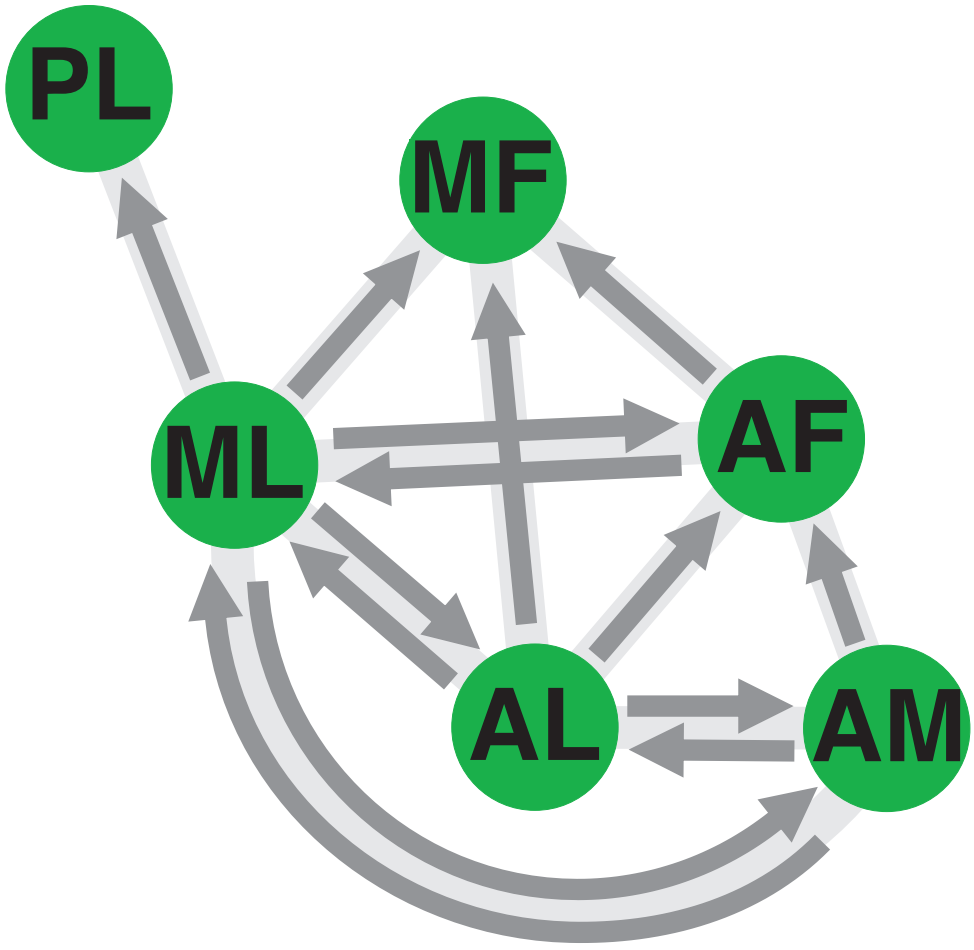


Figure S12: the internal connectivity of the face patch system

**Fig. S1.** Face selective patches in monkeys M2, M3, and M4. Same conventions as in Fig. 1. Flatmaps and timecourses are shown for the hemisphere used for microstimulation. **(A, D, G)** Monkey M2: This animal lacked an AF in the right hemisphere. **(B, E, H)** Monkey M3: This animal showed a full set of six discrete face patches in both hemispheres. **(C, F, I)** Monkey M4: This animal showed a full set of six discrete face patches in the left hemisphere. In the right hemisphere, PL and ML were confluent.

**Fig. S2.** Robustness of the activation pattern to stimulation in ML of monkey M1. Same conventions as Fig. 2C. **(A-D)** Areas activated by microstimulation versus no microstimulation, at four different significance thresholds. **(E, F)** Areas activated by microstimulation versus no microstimulation, for two separate scan sessions.

**Fig. S3.** Brain regions activated by microstimulation in the lateral middle face patch (ML) of monkeys M2 and M3. Same conventions as Fig. 2. **(A-E)** Monkey M2: Since the slice prescription for the initial experiments did not include PL, the experiment was repeated with a more posterior slice prescription. Results from this experiment are shown in the blue inset. Stimulation in ML of this animal produced activity in PL, MF, and AL. Judging from the slice data (D), the two patches of activation in the OTS and upper STS are likely due to blurring of activity at the stimulation site itself and therefore spurious. **(F-J)** Monkey M3: Stimulation produced activity in ML, PL, and AL.

**Fig. S4.** Contralateral cortical activation elicited by microstimulation in the lateral middle face patches (ML) of monkeys M1 and M2. **(A)** In monkey M1, microstimulation in ML produced activation in two contralateral face patches, PL and MF. **(B)** In monkey M2, microstimulation in ML produced activation in contralateral ML (PL was not included in the slice prescription for this experiment). **(C, D)** The same contrast (microstimulation versus no microstimulation) shown on coronal slices (C, monkey M1; D, monkey M2). In

both monkeys the ipsilateral effects of microstimulation were stronger and extended over longer distances than the contralateral effects. **(E, F)** Time courses from the contralateral face patches that were activated in monkey M1 (E) and M2 (F).

**Fig. S5.** Brain regions activated by microstimulation in the left hemisphere lateral anterior face patch (AL) of monkey M4. Same conventions as Fig. 2. Stimulation produced activity in ML, MF, AL, and AM.

**Fig. S6.** Brain regions activated by microstimulation in the ventro-medial anterior face patch (AM) of monkeys M1 and M2. Same conventions as Fig. 2. **(A, F)** Electrode position in AM. **(B, G)** Examples of neuronal selectivity. **(C, H)** In M1, stimulation in AM produced specific activity in ML, AL, and AF. The small region of activation next to AM likely represents spread around the stimulation site that was displaced due to increased susceptibility artifacts from the electrode at this position. In M2, AM stimulation produced specific activity in AL and ML. The slice prescription for M2 excluded PL, so possible activation of this patch could not be observed. The blue inset shows data from the same experiment at lower threshold (the activation in ML was not visible at higher thresholds). **(D, I)** Activation overlaid on coronal slices. PL and MF were the only two face patches that did not show activity modulation by microstimulation. In M1, note activation in the pulvinar (AP position +2.5) and lateral amygdala and claustrum (AP position +17.5). **(E, J)** Time courses from face patches.

**Fig. S7.** Brain regions activated by microstimulation in the anterior face patch in the fundus of the STS (AF) in monkey M1. Same conventions as Fig. 2. **(A)** Electrode position in AF. **(B)** Example of neuronal selectivity. **(C)** Microstimulation in AF produced a spread of activation around the electrode tip, as well as strong activation of MF and weak activation of ML. **(D)** Activation map overlaid on coronal slices. **(E)** Time courses from the six face patches.

**Fig. S8.** Brain regions activated by microstimulation outside the lateral middle face patch (ML) of monkey M2. Same conventions as Fig. 2. **(A)** Electrode position posterior to ML. **(B)** Example of neuronal selectivity. Units recorded at the stimulation site had no clear preference for any of the eight image categories. **(C)** Microstimulation at this site produced a spread of activation around the electrode tip that included PL, but excluded all the other face patches. Note the discrete patch of activation anterior to ML and posterior to AL. **(D)** Activation map overlaid on coronal slices. **(E)** Time courses from PL, ML, and the patch anterior to ML.

**Fig. S9.** Brain regions activated by microstimulation outside AM of monkey M2. Same conventions as Fig. 2. **(A)** Electrode position lateral to AM and medial to AL. **(B)** Microstimulation at this site produced activation around the electrode tip (which was likely shifted posterior due to increased susceptibility artifacts from the electrode at this position), as well as two discrete patches of additional activity. **(C)** Activation map overlaid on coronal slices.

**Fig. S10.** A large swath of cortex is activated by microstimulation in the upper bank of the STS (monkeys M1 and M2). **(A, F)** Electrode position in the upper bank of the STS in area TPO. **(B, G)** Activation for the contrast microstimulation versus no microstimulation, overlaid on the inflated right hemisphere (outlines of the face patches in green). Anatomical labels: *sts:* superior temporal sulcus, *sf:* Sylvan fissure, *cs:* central sulcus, *as:* arcuate sulcus, *cgs:* cingulate sulcus, *cas:* calcarine sulcus, *ots:* occipitotemporal sulcus. **(C, H)** A medial view of the same data, revealing activation of cingulate cortex and adjacent somatosensory and supplementary motor areas. **(D, I)** The same activation overlaid on coronal slices. Posterior area TPO is indicated by black outlines; anterior cingulate cortex by cyan outlines for both monkeys. **(E, J)** Time courses from activated areas. Note the strong modulation in anterior cingulate cortex, despite its considerable distance from the stimulation site.

**Fig. S11.** Microstimulation of face patches activates the amygdala, claustrum, and pulvinar. **(A, B)** Microstimulation in AM of monkeys M1 and M2 produced activity in the ipsilateral lateral amygdala and adjacent claustrum. **(C)** Microstimulation of the lateral middle face patch (ML) in monkey M1 produced strong activity in the ipsilateral inferior pulvinar. **(D)** The inferior pulvinar was also activated by microstimulation in an anterior face patch (AL) in monkey M2. Anatomical labels: lateral amygdala (LA), inferior pulvinar (PI), lateral pulvinar (PL), medial pulvinar (PM). Subcortical area boundaries (black traces) adapted from Ref. 20; in the absence of histological confirmation, these should be regarded as tentative.

**Fig. S12.** The internal connectivity of the face patches. This schematic summarizes the results of all the experiments in the four monkeys (see also Table S2). For each of the four stimulated patches, arrows point to co-activated patches. Note that since MF and PL were not targeted for microstimulation, no arrows leave these patches.

| Experiment | Number of Runs Included in Analysis | | | |
|---|---|---|---|---|
| | M1 | M2 | M3 | M4 |
| face localizer | 15 | 18 | 35 | 23 |
| stimulation in ML | 44 | 64 | 20 | |
| stimulation in AL | 22 | | | 13 |
| stimulation in AM | 22 | 27 | | |
| stimulation in AF | 19 | | | |
| stimulation outside ML | 24 | 22 | | |
| stimulation outside AM | | 14 | | |
| stimulation in upper STS | 19 | 27 | | |
| visual + microstimulation | 29 | 30 | | |

Supplementary Table 1. Summary of Experiments

| Stimulation site | Projection Site | | | | | | |
|---|---|---|---|---|---|---|---|
| | ID | PL | ML | MF | AL | AF | AM |
| ML | M1 | +++ | +++ | +++ | +++ | +++ | ++ |
| | M2 | ++ | +++ | +++ | +++ | n. a. | - |
| | M3 | +++ | +++ | - | +++ | - | - |
| AL | M1 | - | +++ | ++ | +++ | +++ | + |
| | M4 | - | +++ | ++ | +++ | - | + |
| AF | M1 | - | + | +++ | - | +++ | - |
| AM | M1 | - | ++ | - | +++ | +++ | + |
| | M2 | - | + | - | +++ | n. a. | +++ |

n. a.: face patch could not be localized in this monkey
-: no projection detected
+: weak projection detected
++: intermediate projection detected
+++: strong projection detected

Supplementary Table 2. Summary of Results

**Table S1.** Summary of experiments performed in monkeys M1 – M4. Each box indicates the total number of runs that were analyzed to generate the figure for that experiment.

**Table S2.** Summary of results from microstimulating the four face patches in monkeys M1 – M4.

## References


1. D. Y. Tsao *et al.*, *Neuron* **39**, 555 (Jul 31, 2003).
2. D. Y. Tsao, W. A. Freiwald, T. A. Knutsen, J. B. Mandeville, R. B. Tootell, *Nat Neurosci* **6**, 989 (Sep, 2003).
3. D. Y. Tsao, W. A. Freiwald, R. B. H. Tootell, M. S. Livingstone, *Science* **311**, 670 (2006).
4. D. Wegener, W. A. Freiwald, A. K. Kreiter, *J Neurosci* **24**, 6106 (Jul 7, 2004).
5. K. Nelissen, W. Vanduffel, G. A. Orban, *J Neurosci* **26**, 5929 (May 31, 2006).
6. F. P. Leite *et al.*, *Neuroimage* **16**, 283 (Jun, 2002).
7. W. Vanduffel *et al.*, *Neuron* **32**, 565 (Nov 20, 2001).
8. R. Cusack, M. Brett, K. Osswald, *Neuroimage* **18**, 127 (Jan, 2003).
9. H. Zeng, R. T. Constable, *Magn Reson Med* **48**, 137 (Jul, 2002).
10. D. H. Brainard, *Spat Vis* **10**, 433 (1997).
11. R. W. Cox, J. S. Hyde, *NMR Biomed* **10**, 171 (Jun-Aug, 1997).